Chapter 6
The Artistic Geometry of Consensus Protocols

Panagiotis Tsiotras and Luis Ignacio Reyes Castro

Mighty is geometry; joined with art, resistless.
Euripides (480–406 BC)

6.1 The Role of Geometric Patterns in the History of Art

The use of geometric patterns in art has a long history. The geometric period of ancient Greek art (ca. 900–700 BC) is characterized by the extensive use of geometric motifs, mainly on vase and amphorae painting. These decorative motifs (meanders, triangles, circles, etc.) extend horizontally in multiple bands about the vase circumference, and they exhibit central and translational symmetry [7, 18, 45]. Elaborate symmetric geometric patterns also appear extensively in Islamic art, largely due to their aniconic quality [10, 11]. Influenced by previous classical Greek, Roman, and Sasasian works, and fueled by the intellectual contributions of Islamic mathematicians, astronomers, and scientists of the time, Islamic artists created this unique new style, which is characterized by repeated combinations and duplications of simple geometric forms (such as circles and the squares), arranged in intricate, interlaced geometric ornamentations whose complexity is ever increasing, offering the possibility of infinite growth [15]. The exploration of infinity and symmetric growth has also been explored by many subsequent artists. The Dutch graphic artist M. C. Escher (1898–1972) is most famous for his exploration of infinity and of his creations of

P. Tsiotras (✉)
Daniel Guggenheim School of Aerospace Engineering, Georgia Institute of Technology, Atlanta, GA 30332-0150, USA
e-mail: tsiotras@gatech.edu

L. I. R. Castro
Currently a graduate student at the Department of Aeronautics and Astronautics, Massachusetts Institute of Technology, Cambridge, MA 02139, USA

A. LaViers and M. Egerstedt (eds.), *Controls and Art*,
DOI: 10.1007/978-3-319-03904-6_6,

Fig. 6.1 The Irish Trinity Knot (triquetra) consisting of the intersection of three trochoidal-like curves, appears often in medieval Celtic art [38]

impossible images in graphic art [43]. His work on infinite tessellations involving repetitive symmetric patterns on the plane has apparently been heavily influenced by the work of mathematician George Polya (1887–1985) on plane symmetry groups. Escher studied Polya's 17 plane symmetry groups, which led him to develop a mathematical approach to expressions of symmetry, which he later incorporated in his art works. Escher's works primarily exploit planar symmetry groups, otherwise known as "wallpaper designs."

In this chapter we will be dealing with similar geometric planar patterns, which, however, exhibit circular/point symmetry as opposed to regular horizontal/vertical plane symmetry. The interested reader is referred to the seminal work of H. Weyl (1885–1955) [54] for an in-depth discussion on symmetry and symmetry groups. Reference [9] also provides a nice classification of all symmetry groups in one, two, and three dimensions.

We will investigate the generation of highly stylized geometric patterns morphed by repeated repetitions of trochoidal curves on flat or curved surfaces, such as those shown in Fig. 6.2. Trochoidal curves have been in the center of study by several scientists, and are the main focus of our work. They include cycloids, ellipses (and circles), epitrochoids, hypotrochoids, as well as cardioids, astroids, limaçons, and all polar coordinate roses [16]. Although ancient Greeks had discovered trochoids (for instance, the epicycloid had been used by ancient Greeks to describing the movement of the planets long before N. Copernicus (1473–1543) and J. Kepler (1571–1630) established the correct view of heliocentric planet movement in the heavens), the use of trochoids in art seems to have been limited, except in architecture. For example, the Persian astronomer and mathematician Nasir Al-Din al-Tusi (1201–1274) studied the two-cusped hypocycloid [34].

Trochoidal-like curves also appear in Western medieval art. The triquetra symbol (also known as the Irish Trinity Knot), which is usually illustrated as the intersection of three vesicae piscis shapes, appears often in Celtic artwork (Fig. 6.1). This symbol is also prominently depicted in the U-937 runestone, which is one of the four Funbo Runestones, and has been attributed to the 11th century runemaster Fot [41].

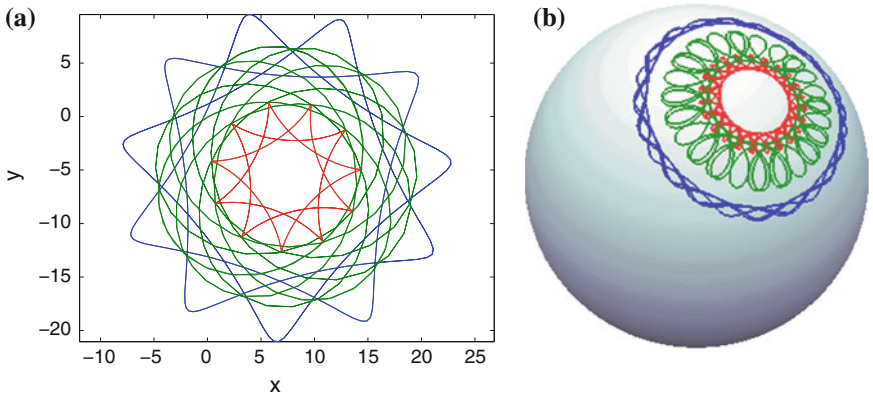

Fig. 6.2 The trochoidal family of curves, which includes cycloids, epitrochoids, hypotrochoids, cardioids, astroids, and limaçons, is the main focus of our work. Trochoids have been studied by several scientists and artists. **a** Interlace of three *trochoidal curves* on the *plane*. **b** Interlace of three *trochoidal curves* on the *sphere*

It is the German artist of the sixteenth century Albrecht Dürer (1471–1528), however, who is credited to be the first to have incorporated trochoids (specifically, hypotrochoidal curves) in his art [47]. He introduced the hypocycloid curve along with the more general family of trochoid curves, in his 1,525 four-volume geometry treatise *The Art of Measurement with Compass and Straightedge*. After Dürer, purely trochoidal curves seem to have been absent from the artistic world up until the invention of the *spirograph* by English engineer Denys Fisher (1918–2002), introduced during the 1965 Nuremberg International Toy Fair. The introduction of the spirograph has created a momentum in the use of trochoidal curves in the Pop Art, Op Art, and Psychedelic Art movements since the 1960s, with several American and European artists incorporating them into their works. Perhaps the first artist in this new line of trochoid admirers is Seattle-based painter Jeffrey Simmons (1968–), who conceived a seven-painting collection titled *Trochoid* [46]. These paintings rely on large hypotrochoids as central features, and were produced with the use of a special-purpose device constructed by the artist himself. English artists Ian Dawson (1969–) and Lesley Halliwell (1965–), also make use of trochoids, although using a very different technique [8, 17]. In their work, they create large colorful shapeless compositions by putting together large numbers of hypotrochoids generated using spirographs. The same technique has also been utilized by Pittsburgh-based illustrator David Pohl, who has used the spirograph as a tool to explore the recurring theme of repetition as a means to illustrate the cyclical nature of life [37]. The American architect Louis Kahn (1901–1974) has also used cycloids in his design of the Kimbell Art Museum [35].

6.2 A Brief of Consensus Protocols

In this chapter, we show how elaborate patterns that are closely related to trochoidal curves can be generated as the paths followed by a team of interacting agents moving on the plane. In the literature of multi-agent control systems, problems involving the coordination of a team of agents such as flocking, swarming, etc., are referred to as consensus problems, and the underlying control strategies enforcing team coordination are commonly referred to as consensus protocols.

Consensus problems have been extensively used for many years in the area of distributed computing and management science. Their recent popularity in the controls community stems from their utilization in formulating and solving a variety of multi-agent, mobile network problems [32, 40]. In this chapter, we propose a generalization of the standard consensus algorithm used widely in the literature [12, 27, 31], and we show how this algorithm can be utilized to generate intricate geometrical patterns for the ensuing agent paths. Using minimal assumptions, the proposed feedback control is able to generate geometric patterns for the agent trajectories that go beyond formation-type geometric models, which deal mainly with identical agents in cycle pursuit [21, 25, 36, 49].

Our inspiration comes from gyroscopic control strategies used in the wheeled robotics community [52] for obstacle avoidance. Since the proposed control law introduces circulation in the underlying vector field, it cannot be derived from a scalar potential, and hence it does not belong to the family of consensus control laws that are gradient-based. As an added benefit of the proposed extension, it is shown that this control law results in consensus points that lie outside the convex hull of the initial positions of the agents. This may be useful for obstacle avoidance and/or consensus with deception, for instance.

As a direct consequence of the proposed extended consensus protocol, in the second part of this chapter we particularize this control law to the case of periodic and quasi-periodic pattern generation, and show how it can be used to generate elaborate, esthetically beautiful patterns.

6.3 Motivating Example

In order to demonstrate the main idea, we start with the simplest of cases, namely, two agents ($N = 2$) in the plane. The extension to the case of an arbitrary number of agents follows readily from this case and it is given in the next section, along with the stability analysis of the overall system with all interacting agents. To this end, assume a given global coordinate frame $\mathcal{E}$ with origin O and two agents at locations $\boldsymbol{r}_1$ and $\boldsymbol{r}_2$, respectively. The kinematic equation for each agent is given by

$$\dot{\boldsymbol{r}}_i = \boldsymbol{u}_i, \qquad i = 1, 2. \tag{6.1}$$

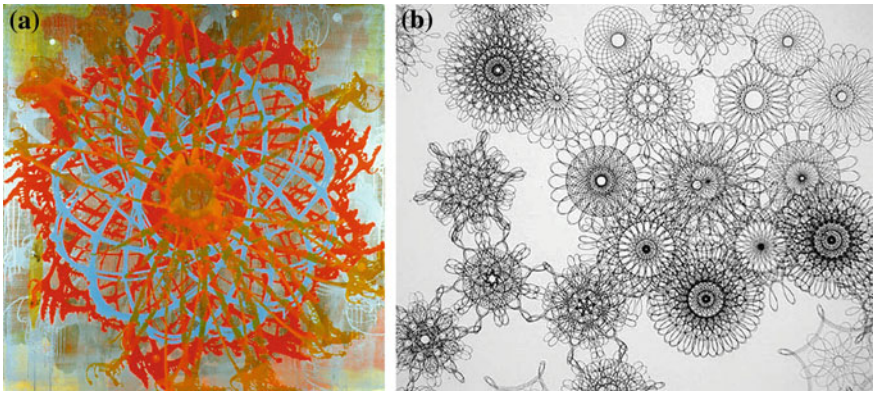

Fig. 6.3 Several modern artists have experimented with the use of trochoidal curves in their work. **a** Warmth of the Sun (1999). Oil and alkyd on canvas by J. Simmons. (Reprinted with permission [46]). **b** A80 (2000). Ink on gesso on primed board by I. Dawson. (Reprinted with permission [8])

We assume that only the *relative* distance $\boldsymbol{r}_{12} = \boldsymbol{r}_1 - \boldsymbol{r}_2$ is known to agent no. 1 and, similarly, only the relative distance $\boldsymbol{r}_{21} = -\boldsymbol{r}_{12}$ is available to agent no. 2. It can be easily shown [27] that the control law

$$\boldsymbol{u}_1 = -\gamma_1 \boldsymbol{r}_{12}, \qquad \boldsymbol{u}_2 = -\gamma_2 \boldsymbol{r}_{21}, \qquad \gamma_1 + \gamma_2 > 0 \tag{6.2}$$

achieves consensus. That is, the distance between the two agents will tend to be zero as the time progresses. Furthermore, with the control law in (6.2), the two agents will meet somewhere along the line segment initially connecting $\boldsymbol{r}_1(0)$ and $\boldsymbol{r}_2(0)$. Our first objective is to modify (6.2) in order to allow convergence of the agents to points that do not necessarily belong to the line segment (in general, the convex hull) defined by the initial position vectors.

The main observation here is that the control law (6.2) does not make use of all available geometric information to each agent. For instance, agent no. 1 knows not only the vector $\boldsymbol{r}_{12}$ but also all vectors (directions) *perpendicular* to $\boldsymbol{r}_{12}$, which can then be used in a feedback strategy. Similarly, for agent no. 2, this additional information in the control law, inferred from—but distinct than—the relative position vector between the agents, can lead to more flexibility for trajectory design. To this end, let $\boldsymbol{q}_{12}$ and $\boldsymbol{q}_{21}$ be such that $\boldsymbol{q}_{12} \cdot \boldsymbol{r}_{12} = \boldsymbol{q}_{21} \cdot \boldsymbol{r}_{21} = 0$, and assume the following control laws[1]

$$\boldsymbol{u}_1 = -\gamma_1 \boldsymbol{r}_{12} + \beta_1 \boldsymbol{q}_{12}, \qquad \boldsymbol{u}_2 = -\gamma_2 \boldsymbol{r}_{21} + \beta_2 \boldsymbol{q}_{21} \tag{6.3}$$

Later, it will be shown that this control law also achieves consensus for $\gamma_1 + \gamma_2 > 0$ and $\beta_1, \beta_2 \in \mathbb{R}$.

[1] Owing to the freedom in choosing $\boldsymbol{q}_{12}$ and $\boldsymbol{q}_{21}$, we define a "position orientation" such that $\boldsymbol{r}_{12} \times \boldsymbol{q}_{12} = \boldsymbol{r}_{21} \times \boldsymbol{q}_{21}$.

In preparation for the general case, let us now introduce coordinates, with respect to a global frame $\mathcal{E}$, leading to $[\boldsymbol{r}_i]_{\mathcal{E}} \triangleq x_i \in \mathbb{R}^2$, $(i = 1, 2)$ and $[\boldsymbol{r}_{12}]_{\mathcal{E}} = [\boldsymbol{r}_1]_{\mathcal{E}} - [\boldsymbol{r}_2]_{\mathcal{E}} = x_1 - x_2$. Let the error vector $z \in \mathbb{R}^2$ of the relative distance between the two agents be

$$z \triangleq x_1 - x_2 = d_{11}x_1 + d_{21}x_2 = (D^{\mathsf{T}} \otimes I_2)x, \tag{6.4}$$

where $D = \begin{bmatrix} 1 & -1 \end{bmatrix}^{\mathsf{T}}$ and where $x = [x_1^{\mathsf{T}},\ x_2^{\mathsf{T}}]^{\mathsf{T}} \in \mathbb{R}^4$. Furthermore, let $[\boldsymbol{q}_{12}]_{\mathcal{E}} \triangleq p = Sz$ where S is the skew symmetric matrix

$$S = \begin{bmatrix} 0 & -1 \\ 1 & 0 \end{bmatrix}. \tag{6.5}$$

It is clear that $p^{\mathsf{T}}z = z^{\mathsf{T}}p = 0$. It can then be easily seen that the control law (6.3) can be written compactly, as follows

$$\begin{aligned} u &= -(\Gamma \otimes I_2)(D \otimes I_2)z + (B \otimes I_2)(D \otimes I_2)Sz \\ &= -(\Gamma D \otimes I_2)z + (BD \otimes S)z, \end{aligned} \tag{6.6}$$

where $u = [u_1^{\mathsf{T}},\ u_2^{\mathsf{T}}]^{\mathsf{T}} \in \mathbb{R}^4$ and $\Gamma = \operatorname{diag}(\gamma_1, \gamma_2)$ and $B = \operatorname{diag}(\beta_1, \beta_2)$. From (6.4) it follows that the error equation is given by

$$\begin{aligned} \dot{z} &= (D^{\mathsf{T}} \otimes I_2)\dot{x} = (D^{\mathsf{T}} \otimes I_2)u \\ &= -(D^{\mathsf{T}} \otimes I_2)(\Gamma \otimes I_2)(D \otimes I_2)z + (D^{\mathsf{T}} \otimes I_2)(B \otimes I_2)(D \otimes I_2)Sz \\ &= -\Big(\big(D^{\mathsf{T}}\Gamma D\big) \otimes I_2\Big)z + \Big(\big(D^{\mathsf{T}}BD\big) \otimes S\Big)z. \end{aligned}$$

Stability is determined by the eigenvalues of the matrix $A_{\mathrm{CL}} = -\big((D^{\mathsf{T}}\Gamma D) \otimes I_2\big) + \big((D^{\mathsf{T}}BD) \otimes S\big)$. A simple calculation shows that $\operatorname{spec}(A_{\mathrm{CL}}) = \{-(\gamma_1 + \gamma_2) \pm \mathrm{i}(\beta_1 + \beta_2)\}$. Hence consensus is achieved asymptotically as long as $\gamma_1 + \gamma_2 > 0$. The "classical" consensus control law (6.2) corresponds to the case when $\beta_1 = \beta_2 = 0$. When $B \neq 0$ stability is still maintained, however, the transient response is different. Furthermore, the point where consensus is achieved can be selected to lie outside the line segment connecting $x_1(0)$ and $x_2(0)$ by a proper choice of the gains β_1 and β_2. This is demonstrated in Fig. 6.4 where the result of a simulation with the data $x_1(0) = (-1, 1)^{\mathsf{T}}$, $x_2(0) = (2, 3)^{\mathsf{T}}$, $\Gamma = \operatorname{diag}(0.1, 1)$, $B = \operatorname{diag}(-0.5, 2)$ is shown. For this example the two agents meet at the point with coordinates $(-2, 1)$.

6.4 Extension to N Agents in the Plane

For the general case, consider N agents in the plane. Assume that their location is given by the state variables $x_i \in \mathbb{R}^2$ for $i = 1, \ldots, N$, expressed in the same, common global frame $\mathcal{E}$, satisfying the differential equations

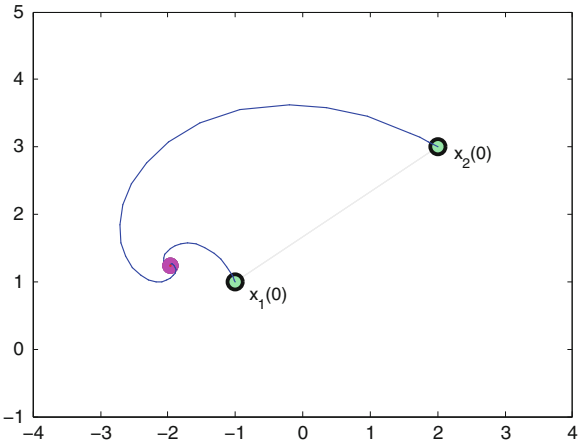

Fig. 6.4 Numerical example with "skew-symmetric" feedback. The skew-symmetric term creates a vector field with circulation

$$\dot{x}_i = u_i, \qquad i = 1, \ldots, N. \tag{6.7}$$

To the N agents we associate a graph $\mathcal{G}$ that describes the communication topology between the agents. That is, $\mathcal{G}$ has N nodes and M edges (links), with each edge denoting knowledge of the relative position between the corresponding agents. We can define the incidence matrix $D \in \mathbb{R}^{N\times M}$ with elements as follows [1]. We assign $d_{ij} = +1$ (-1) if the ith node is the head (tail) of jth edge, and $d_{ij} = 0$ otherwise. If the ith agent is a neighbor with the jth agent, then they are connected by an edge, and we have the difference (error) variable

$$z_k = \sum_{\ell=1}^{N} d_{\ell k} x_\ell = \begin{cases} x_i - x_j, & \text{if } i \text{ is the head,} \\ x_j - x_i, & \text{if } j \text{ is the head,} \end{cases} \tag{6.8}$$

where $z_k \in \mathbb{R}^2$ for $k = 1, \ldots, M$. If the columns of D are linearly independent, that is, if the graph does not contain cycles, then the vectors z_k are linearly independent [1]. Note also that the graph is connected if and only if rank $D = N - 1$ [14, 31]. Introducing the stack vector $x = \left[x_1^\mathsf{T} \cdots x_N^\mathsf{T}\right]^\mathsf{T} \in \mathbb{R}^{2N}$, the state equations (6.7) can be written compactly as

$$\dot{x} = u, \tag{6.9}$$

where $u = \left[u_1^\mathsf{T} \cdots u_N^\mathsf{T}\right]^\mathsf{T} \in \mathbb{R}^{2N}$. Following (6.6), we propose the control law

$$u = -(\Gamma D \otimes I_2)z + (BD \otimes S)z, \tag{6.10}$$

where $z = \left[z_1^\mathsf{T} \cdots z_M^\mathsf{T}\right]^\mathsf{T} \in \mathbb{R}^{2M}$, and where $\Gamma = \text{diag}(\gamma_1, \ldots, \gamma_N)$ and $B = \text{diag}(\beta_1, \ldots, \beta_N)$. The standard consensus algorithm results as a special case of (6.10) where $B = 0$.

Convergence Analysis

From (6.8) it can be easily shown that the error vector z can be written compactly as follows

$$z = (D^\mathsf{T} \otimes I_2)x. \tag{6.11}$$

From (6.10) the differential equation for x is then given by

$$\begin{aligned} \dot{x} &= -(\Gamma D \otimes I_2)(D^\mathsf{T} \otimes I_2)x + (BD \otimes S)(D^\mathsf{T} \otimes I_2)x \\ &= -\big((\Gamma DD^\mathsf{T}) \otimes I_2 - (BDD^\mathsf{T}) \otimes S\big)x \\ &= -\big((\Gamma L) \otimes I_2 - (BL) \otimes S\big)x, \end{aligned} \tag{6.12}$$

where $L \triangleq DD^\mathsf{T} \in \mathbb{R}^{N\times N}$ is the *graph Laplacian* [27]. Let $\mathbf{1}_N \triangleq (1, 1, \ldots, 1)^\mathsf{T} \in \mathbb{R}^N$ denote the N-dimensional column vector of ones, and recall that $L\mathbf{1}_N = 0$ [14, 27]. For any $v \in \mathbb{R}^2$ we have that $\big((\Gamma L)\otimes I_2 - (BL)\otimes S\big)(\mathbf{1}_N \otimes v) = (\Gamma L\mathbf{1}_N)\otimes v - (BL\mathbf{1}_N)\otimes(Sv) = 0$. It follows that the vector $\mathbf{1}_N \otimes v$ spans the null space of the matrix in (6.12). The equilibrium point $\bar{x}_\infty$ of the linear differential equation (6.12) therefore satisfies the condition $\bar{x}_\infty \triangleq \lim_{t\to\infty} x(t) = \mathbf{1}_N \otimes x_\infty$ for some $x_\infty \in \mathbb{R}^2$, from which it follows that $\lim_{t\to\infty} x_1(t) = \lim_{t\to\infty} x_2(t) = \cdots = \lim_{t\to\infty} x_N(t) = x_\infty$, thus achieving consensus.

Let the coordinates of the final consensus point be $x_\infty = [\mathsf{x}_\infty\ \mathsf{y}_\infty]^\mathsf{T} \in \mathbb{R}^2$. We have the following proposition.

Proposition 1 [51]. *Let* $v_1, v_2 \in \mathbb{R}^{2N}$ *be such that* $\text{span}\{v_1, v_2\} = \mathcal{R}^\perp\big((\Gamma L) \otimes I_2 - (BL) \otimes S\big)$. *The final rendezvous point is given by*

$$x_\infty = \begin{bmatrix} \mathsf{x}_\infty \\ \mathsf{y}_\infty \end{bmatrix} = \begin{bmatrix} v_1^\mathsf{T}(\mathbf{1}_N \otimes I_2) \\ v_2^\mathsf{T}(\mathbf{1}_N \otimes I_2) \end{bmatrix}^{-1} \begin{bmatrix} v_1^\mathsf{T} x(0) \\ v_2^\mathsf{T} x(0) \end{bmatrix}. \tag{6.13}$$

If $\Gamma = 0$ there is not "rendezvous" point. Instead, the agents follow closed trajectories centered around the point given by equation (6.13).

6.5 Periodic and Quasi-Periodic Trajectories

Given an interconnection topology, the particular choices of the gain matrices Γ and B can be used to generate specific trajectory patterns for the ensuing agent paths. Since we are mainly interested in periodic or quasi-periodic trajectories, next we restrict the discussion to the case $\Gamma = 0$. By letting $\Gamma = 0$ in (6.10) the control law becomes

$$u = (BD \otimes S)z, \tag{6.14}$$

and the closed-loop system reduces to

$$\dot{x} = ((BL) \otimes S)\, x. \tag{6.15}$$

The shape and frequencies of the resulting paths are therefore determined by the eigenvalues and eigenvectors of the matrix $(BL) \otimes S$. Recall from the properties of the Kronecker product [6] that the eigenvalues of the matrix $(BL) \otimes S$ are of the form $\lambda\mu$, where $\lambda \in \text{spec}(BL)$ and $\mu \in \text{spec}\, S$. Additionally, the corresponding eigenvectors are of the form $\mathsf{v} \otimes \mathsf{u}$ where $\mathsf{v} \in \mathbb{C}^3$ is the eigenvector of the matrix BL associated with λ and $\mathsf{u} \in \mathbb{C}^2$ is the eigenvector of the matrix S associated with μ. Since $\det(\lambda I_N - BL) = \det(\lambda I_N - BDD^{\mathsf{T}}) = \det(\lambda I_M - D^{\mathsf{T}}BD)$ it follows that the nonzero eigenvalues of the matrix BL coincide with the nonzero eigenvalues of $D^{\mathsf{T}}BD$. Because the latter matrix is symmetric, all eigenvalues of BL are real. Consequently, all eigenvalues of $(BL)\otimes S$ lie on the imaginary axis. It follows that the solutions of (6.15) consist, in general, of a superposition of sine and cosine functions, perhaps multiplied by polynomials in t (in the case of multiple eigenvalues).

Let $BL = VJV^{-1}$ be the spectral decomposition of the matrix BL. It can be easily shown that

$$\mathrm{e}^{((BL)\otimes S)t} = (V \otimes I_2)\, \mathrm{e}^{(J\otimes S)t}\, (V^{-1} \otimes I_2). \tag{6.16}$$

The spectral decomposition of the matrix BL thus provides all information needed to investigate the nature of the solutions of (6.15). In fact, additional information can be gathered owing to the special structure of the state matrix in (6.15).

Lemma 1. *Let A be an $n \times n$ square matrix and let S be the 2×2 skew-symmetric matrix given in (6.5). Then*

$$\mathrm{e}^{A\otimes S} = \cos A \otimes I_2 + \sin A \otimes S. \tag{6.17}$$

Proof. Notice that $S^{2k} = (-1)^k I_2$ and $S^{2k+1} = (-1)^k S$, $k = 0, 1, 2, \ldots$ and recall that

$$\mathrm{e}^{A\otimes S} = \sum_{k=0}^{\infty} \frac{1}{k!} (A \otimes S)^k.$$

The right-hand side of the previous equation can be expanded as follows

$$\begin{aligned}
&\sum_{k=0}^{\infty} \frac{1}{(2k)!}\big(A \otimes S\big)^{2k} + \sum_{k=0}^{\infty} \frac{1}{(2k+1)!}\big(A \otimes S\big)^{2k+1} \\
&= \sum_{k=0}^{\infty} \frac{1}{(2k)!}\big(A^{2k} \otimes S^{2k}\big) + \sum_{k=0}^{\infty} \frac{1}{(2k+1)!}\big(A^{2k+1} \otimes S^{2k+1}\big) \\
&= \Big(\sum_{k=0}^{\infty} \frac{(-1)^k}{(2k)!} A^{2k}\Big) \otimes I_2 + \Big(\sum_{k=0}^{\infty} \frac{(-1)^k}{(2k+1)!} A^{2k+1}\Big) \otimes S.
\end{aligned}$$

Making use of the fact that for a square matrix A,

$$\cos A = \sum_{k=0}^{\infty} \frac{(-1)^k}{(2k)!} A^{2k}, \quad \sin A = \sum_{k=0}^{\infty} \frac{(-1)^k}{(2k+1)!} A^{2k+1},$$

the result of the lemma follows immediately.

We therefore have the following proposition.

Proposition 2 *The solution of* (6.15) *is given by*

$$\begin{aligned}
x(t) &= \big(\cos(BLt) \otimes I_2 + \sin(BLt) \otimes S\big)x(0), \\
&= (V \otimes I_2)\big(\cos(Jt) \otimes I_2 + \sin(Jt) \otimes S\big)(V^{-1} \otimes I_2)x(0),
\end{aligned} \tag{6.18}$$

for all $t \geq 0$ *and all* $x(0) \in \mathbb{R}^{2N}$.

The structure of the state matrix in (6.15) (e.g., its eigenvalues and eigenvectors) thus can provide a great deal of information regarding the paths followed by the agents in the Cartesian coordinate frame, as well as the relative location of the agents on these paths (i.e., their relative phasing). For instance, one can ensure that the agent trajectories either form closed paths with given phasing, or they form a dense set of trajectories, ensuring that almost every point in a given region will be visited at least once by one or more agents. Such orbits could be desirable, for instance, in surveillance or area coverage applications (see Fig. 6.8). Moreover, as shown in the next section, these orbits are also esthetically appealing. In that respect, geometric beauty serves as a functional element for the solution of meaningful engineering problems.

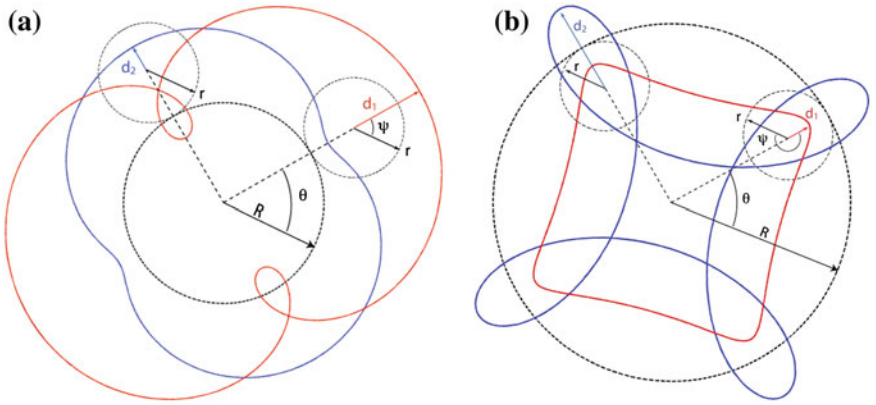

Fig. 6.5 Representative examples of epitrochoids and hypotrochoid curves. **a** *Epitrochoid curves* The *blue curve* has $d < r$, while the second one has $d > r$. Both epitrochoids have $R = 4, r = 2$ (hence $k = 2$). **b** *Hypotrochoid curves* The *blue curve* has $d > r$, while the second one has $d < r$. Both epitrochoids have $R = 6, r = 1.5$ (hence $k = 4$)

6.6 Orbit Pattern Generation

In this section, we show that the solutions of (6.15) result in elaborate geometric trochoidal patterns. As is seen by (6.18), the solutions depend on the gain matrix B, the Laplacian matrix L that encodes the connectivity, as well as the initial conditions $x(0)$.

6.6.1 A Family of Achievable Paths

The solutions in (6.18) fall in the general class of *trochoidal* curves. An *epitrochoid* curve is generated by a point P attached at a radial distance d from the center of a circle of radius r, which is rolling without slipping around a circular track of radius R; see Fig. 6.5a. The distance d can be smaller, equal, or greater than the radius r of the rolling circle. The ratio of the circular two tracks $k = R/r$ indicates the number of points at which the agent is closest to the center of the circular track. These are referred to as *crests*. In the special case when $r = d$, the curve becomes an *epicycloid* with k *cusps*; at these points, the curve is not differentiable. Note that ellipsoidal paths correspond to the case when $k = 0$. A *hypotrochoid* is generated by a point P attached at a distance d from the center of a circle of radius r, which rolls inside a circle of radius R; see Fig. 6.5b. Again, the distance d can be smaller, equal, or greater than the radius r of the rolling circle; this radius, however, cannot exceed that of the circle R.

As mentioned in the introduction, the trochoidal family of curves is very rich and includes many of the well-known curves such as ellipses and circles, (epi/hypo) cycloids, cardioids, limaçons, etc. The most well-known example of a trochoid curve

is the cycloid—the "courbe merveilleuse" of M. Chasles (1793–1880). The cycloid often appears as the solution to many problems in mathematics, physics. For instance, Bernoulli's brachystochrone problem in the Calculus of Variations, and the paths followed by charged particles in crossed electric and magnetic fields turn out to be cycloids. Because of its recurring appearance as the solution of many problems the cycloid has been the center of investigation by several mathematicians, and its study has not escaped controversy. It fact, owing to the many disputes it provoked between mathematicians over the centuries it has been called the "Helen of geometers" [5], in reference to the beautiful Helen of Troy who caused many quarrels among men, and whose abduction by Paris, the son of Priam King of Troy, caused the Trojan War.

In the next section, we investigate a few interesting cases of trochoids resulting from the solution of (6.18).

6.6.2 *Illustrative Example: Three Agents*

In this section, we investigate in greater detail the simple nontrivial case, namely, three agents in the plane ($N = 3$), connected either in a path graph ($M = 2$) or a complete graph ($M = 3$). For a path graph interconnection the incidence matrix is given by

$$D = \begin{bmatrix} -1 & 0 \\ 1 & -1 \\ 0 & 1 \end{bmatrix}. \tag{6.19}$$

A straightforward calculation shows that the two nonzero eigenvalues of the matrix BL for this case are given by

$$\frac{\beta_1}{2} + \beta_2 + \frac{\beta_3}{2} \pm \frac{\sqrt{\beta_1^2 - 2\beta_1\beta_3 + 4\beta_2^2 + \beta_3^2}}{2}.$$

For the complete graph the incidence matrix is given by

$$D = \begin{bmatrix} -1 & 0 & 1 \\ 1 & -1 & 0 \\ 0 & 1 & -1 \end{bmatrix}. \tag{6.20}$$

The nonzero eigenvalues of the matrix BL for this case are given by

$$\beta_1 + \beta_2 + \beta_3 \pm \sqrt{\beta_1^2 + \beta_2^2 + \beta_3^2 - \beta_1\beta_2 - \beta_2\beta_3 - \beta_3\beta_1}.$$

The ratio of the two nonzero eigenvalues is equal to $k + 1$ for an epitrochoid or $k - 1$ for a hypotrochoid. Note that if k turns out to be an irrational number, then the

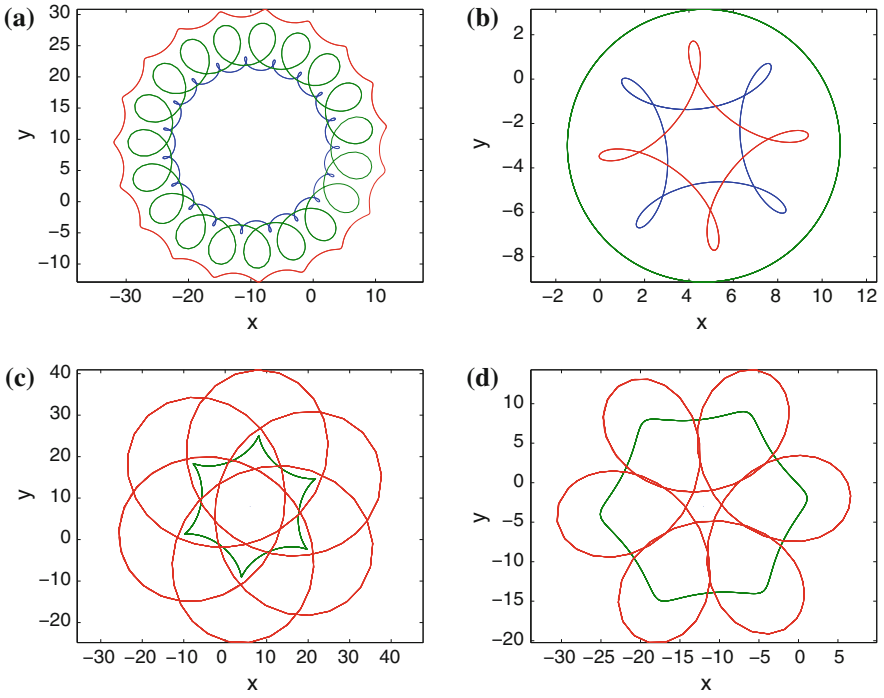

Fig. 6.6 Orbits with three agents using the extended consensus protocol; path graph. **a** $B = \text{diag}(1, 2.0034, -1)$. **b** $B = \text{diag}(-1, 2, -1)$. **c** and **d** $B = \text{diag}(0, 1, -6.5933)$

number of crests is infinite, which means that the curve is not closed; instead, the trajectories form a dense subset of the space [19]. See Figs. 6.6 and 6.7.

An orbit redesign can yield periodic orbits of a particular shape that can be used for coordinated, distributed surveillance, and perimeter monitoring applications; see, for instance, Fig. 6.8. Such an orbit redesign may require a complete interconnection topology [51].

An interesting case occurs when the closed-loop system has two zero eigenvalues at the origin. In this case the trajectories exhibit secular motion. Figure 6.9a shows the trajectories when $B = \text{diag}(0.5, -1, -1)$. It can be easily verified that in this case the relative orbits for the three agents are all circles; see Fig. 6.9b.

There is of course a plethora of possibilities to explore, and one can only imagine the different ways to use the flexibility offered by this serendipitous marriage of art, geometry, and multi-agent control system for solving meaningful, real-world engineering problems.

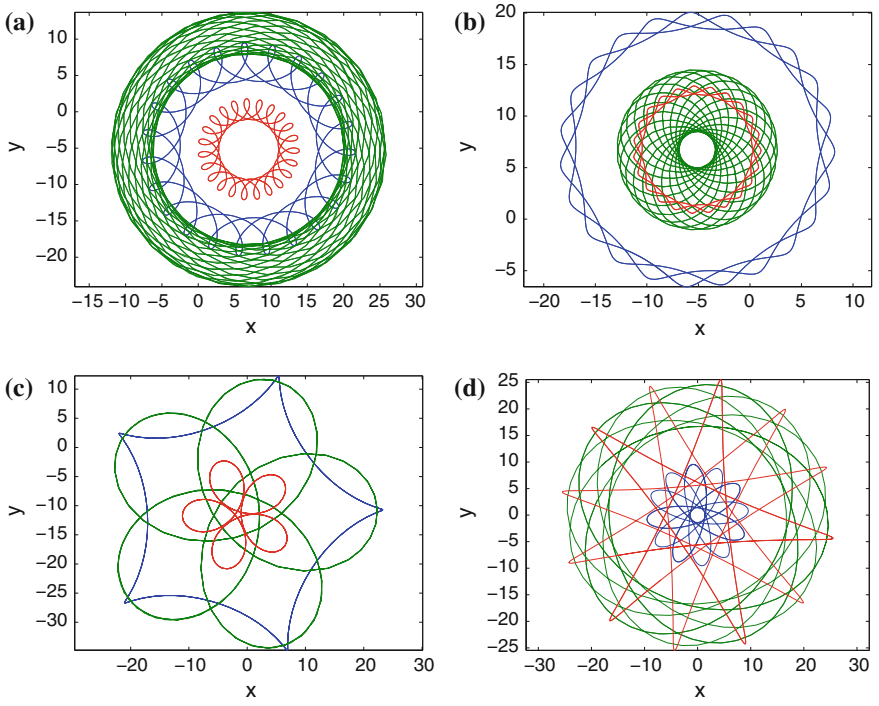

Fig. 6.7 Orbits with three agents using the extended consensus protocol; path graph. **a** and **b** $B = \text{diag}(1, -2.9054, 0.5)$. **c** $B = \text{diag}(1, -1, -0.5)$. **d** $B = \text{diag}(-0.75, 1.67259, -2)$

6.7 A Gallery of Orbits

Using the extended consensus protocols one can clearly generate a myriad of beautiful geometric patterns, by changing the gain matrix B and by choosing a suitable graph Laplacian L in (6.15). Figures 6.6, 6.7, 6.8, 6.9, 6.10, 6.11 and 6.12 provide a glimpse on the plethora and variety of geometric patterns generated using the consensus control law in (6.15) for the case of three and four agents on the plane. We urge the reader to try his/her own skills at generating visually pleasing curves using Eq. (6.15).

In addition to monitoring and surveillance applications already mentioned, these and similar geometric patterns, can also be used in all cases where the resulting motion of a group of agents is to be determined distributively, solely by inter-agent interactions. For instance, they could serve as periodic motion primitives for executing elaborate choreographic patterns for human dancers or small autonomous robotic vehicles, as it is done, for example in the work of Schoelling et al. [44] and Leonard et al. [22] elsewhere in this book. Indeed, one can envision situations where swarm dance patterns—accompanied perhaps by music—can evolve to agents paths resembling those shown in Figs. 6.6, 6.7, 6.8, 6.9, 6.10, 6.11, and 6.12. One needs only to impose the correct communication topology in the underlying graph and the

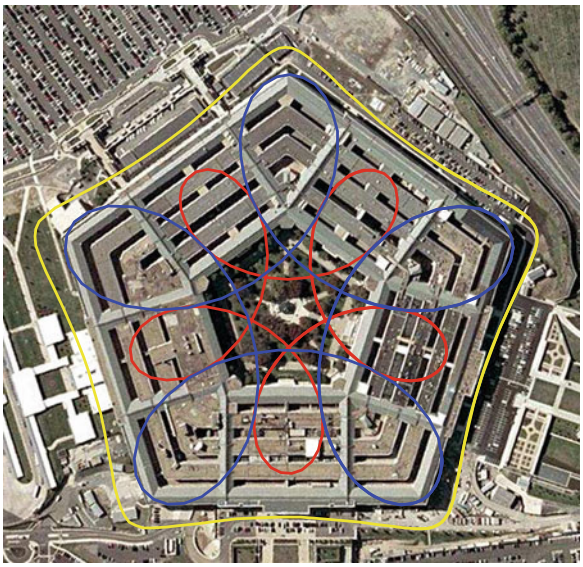

Fig. 6.8 Trochoidal paths that could be used by three agents to patrol a *pentagon-shaped* area. Satellite image courtesy of USGS [39]

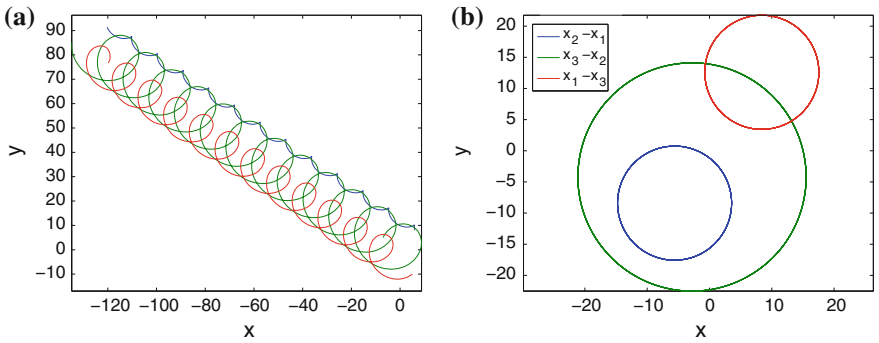

Fig. 6.9 $B = \text{diag}(0.5, -1, -1)$ and initial conditions $x_1(0) = (6, 8)$, $x_2(0) = (-7, 5)$, $x_3(0) = (5, -10)$ (path graph interconnection). The figure on the *right* shows the relative orbits

correct gain weights. Although such an idea may seem intuitive and appealing, we should offer a word of caution: in all our developments so far we have not taken into consideration the case when two agents happen to be at the same location at the same time. That is, collision avoidance is not built-in a priori into (6.15) and, depending on the size of the agents with respect to the size of these orbits, may indeed be a problem during implementation. Along these lines, a much needed future research direction is the design of such geometric patterns for dance or flock formation (or other more

engineering oriented applications such as patrolling or surveillance) while—at the same time—incorporating collision avoidance guarantees.

6.8 Extensions to Pattern Generation on Curved Surfaces

The previous methodology can be easily extended to generate similar intricate trochoidal paths on any two-dimensional manifold. Although the classical consensus protocol has been extended to the case of agents moving on a sphere [30] or a general manifold [42, 50], in this work we will follow an alternative—more direct approach—to generate trochoidal curves on a sphere, by taking advantage of the fact that a two-dimensional manifold is a surface that "locally" looks like a two-dimensional plane. Given therefore a two-dimensional manifold $\mathcal{M}$ (in this case, a sphere, $\mathcal{M} = \mathbb{S}^2$) we can define local coordinates $y_1 = \phi_1(q)$ and $y_2 = \phi_2(q)$, where $q \in \mathcal{M}$, and where $\phi \triangleq (\phi_1, \phi_2) : \mathcal{M} \mapsto \mathbb{R}^2$ is a homeomorphism between an open subset of $\mathcal{M}$ and an open subset of $\mathbb{R}^2$.

Using the spherical coordinates $\phi \in [-\pi, \pi]$ (azimuth) and $\theta \in [-\pi/2, \pi/2]$ (elevation), the equations of any point of the orbit on the unit sphere is given by

$$\mathsf{x} = \cos\theta \cos\phi, \qquad \mathsf{y} = \cos\theta \sin\phi, \qquad \mathsf{z} = \sin\theta. \tag{6.21}$$

Assume now that the equations of motion of each agent on the sphere obey the equations (6.7), where $x_i = (\phi_i, \theta_i)$ are the coordinates for each agent, for $i = 1, \ldots, N$. We again assume that the agents implement the control law

$$u = (BD \otimes I_2)p = (BD \otimes S)z, \tag{6.22}$$

where $p = (I_M \otimes S)z$. Results from implementing this control law for various values of the matrices B and D are shown in Fig. 6.13. Figure 6.13 shows examples of trochoidal patterns on a two-dimensional unit sphere using the formulas (6.21).

Still another alternative approach to generate paths on the sphere is to use the (inverse) stereographic or geodesic projections onto the two-dimensional sphere of a pattern generated by the proposed extended consensus protocol on the plane. Recall that the stereographic projection $\pi_s : \mathbb{S}^2 \backslash \{(0, 0, 1)\} \mapsto \mathbb{R}^2$ is defined via the expressions

$$x = \frac{\mathsf{x}}{1 - \mathsf{z}}, \qquad y = \frac{\mathsf{y}}{1 - \mathsf{z}}, \tag{6.23}$$

for $(\mathsf{x}, \mathsf{y}, \mathsf{z}) \in \mathbb{S}^2$, that is, $\mathsf{x}^2 + \mathsf{y}^2 + \mathsf{z}^2 = 1$. Alternatively, the geodesic projection $\pi_g : \mathbb{S}^2 \backslash \mathbb{S}^1 \mapsto \mathbb{R}^2$ is defined via the expressions

$$x = \frac{\mathsf{x}}{\mathsf{z}}, \qquad y = \frac{\mathsf{y}}{\mathsf{z}}, \tag{6.24}$$

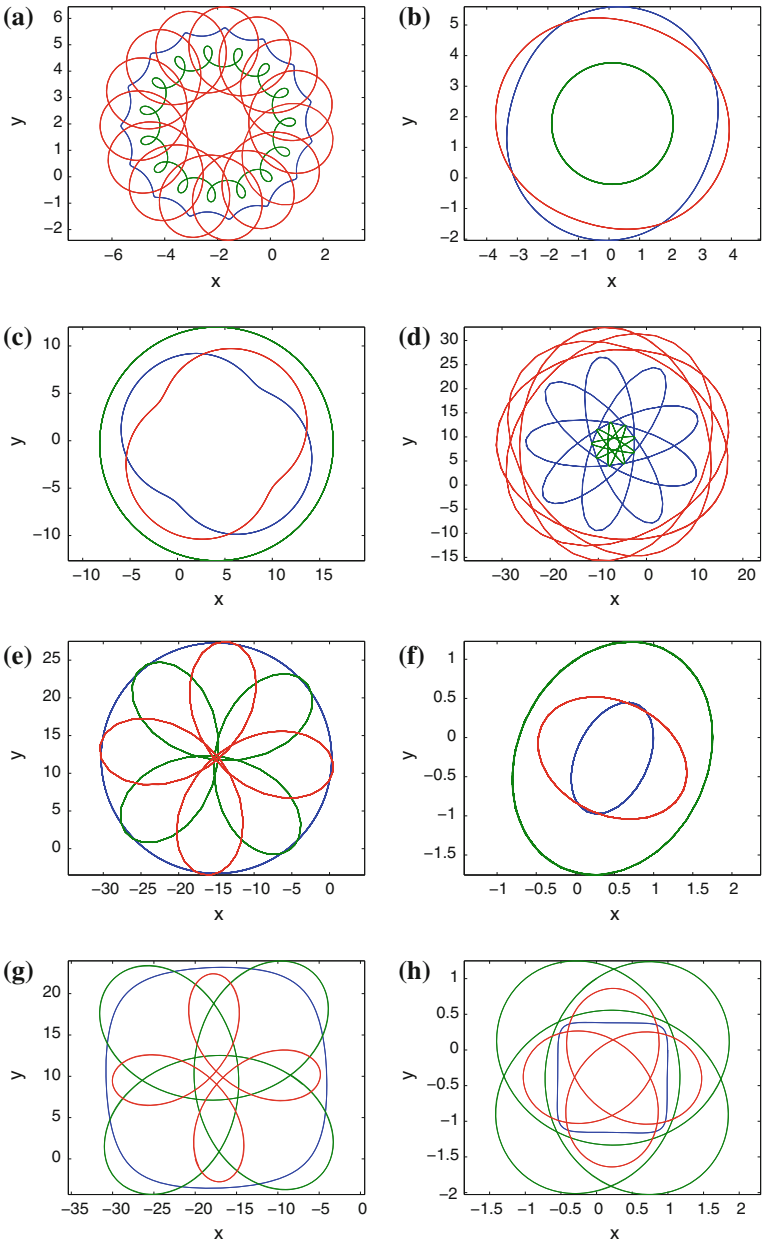

Fig. 6.10 A menagerie of orbits with three agents using the extended consensus protocol; complete graph. **a** $B = \text{diag}(-1, 1, 3)$, **b** and **c** $B = \text{diag}(0.5, 2, 0.5)$, **d** $B = \text{diag}(-1, -0.1936, 1)$, **e** $B = \text{diag}(4, -4, -4)$, **f** $B = \text{diag}(-5, 3, 2)$, **g** and **h** $B = \text{diag}(-2.4736, 3, 2)$

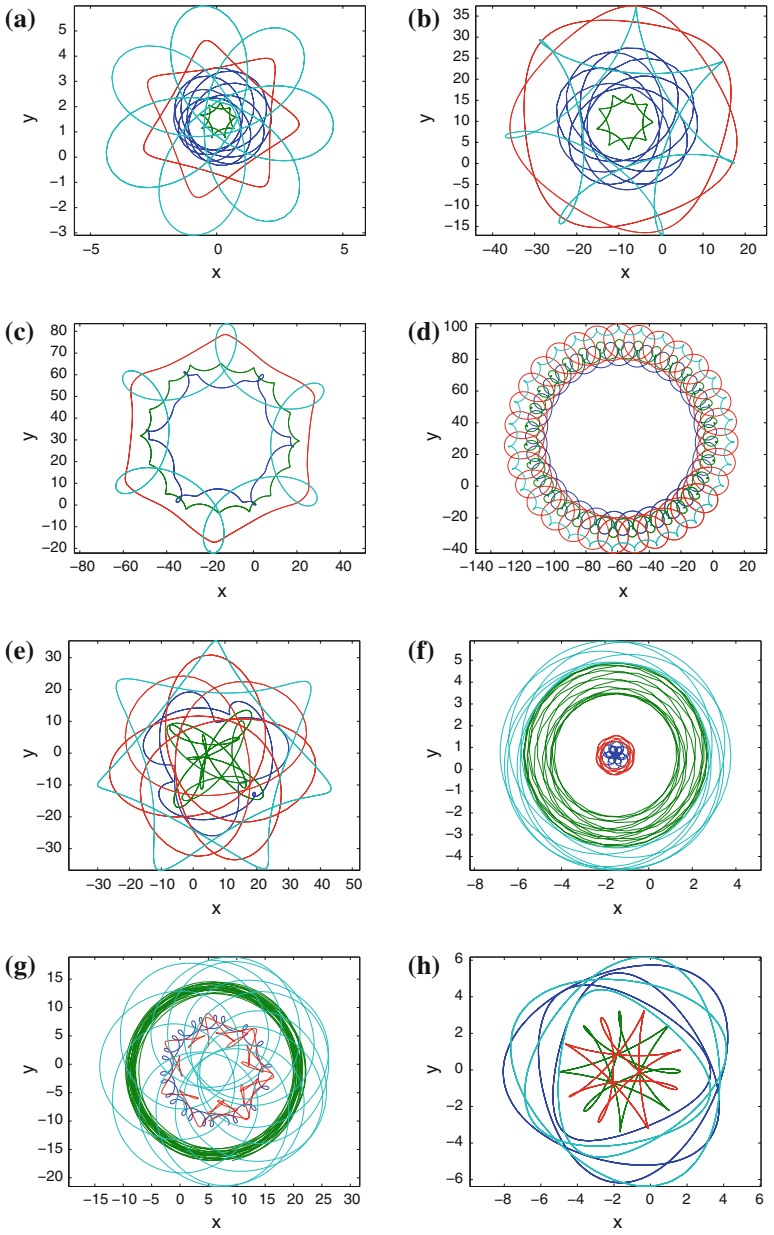

Fig. 6.11 Sample orbits with four agents using the extended consensus protocol; path graph. **a** and **b** $B = \text{diag}(2, 0.1826, -0.6126, 2)$, **c** $B = \text{diag}(2, 1.7141, -0.8257, 2)$, **d** $B = \text{diag}(2, 3.622, 2.336, -1)$, **e** $B = \text{diag}(-1, -1.145, 1.297, -1)$, **f** $B = \text{diag}(0.15, -1, 0.15, -1)$, **g** $B = \text{diag}(0.15, -1, 0.15, 1)$, **h** $B = \text{diag}(5, -2, -2, 5)$

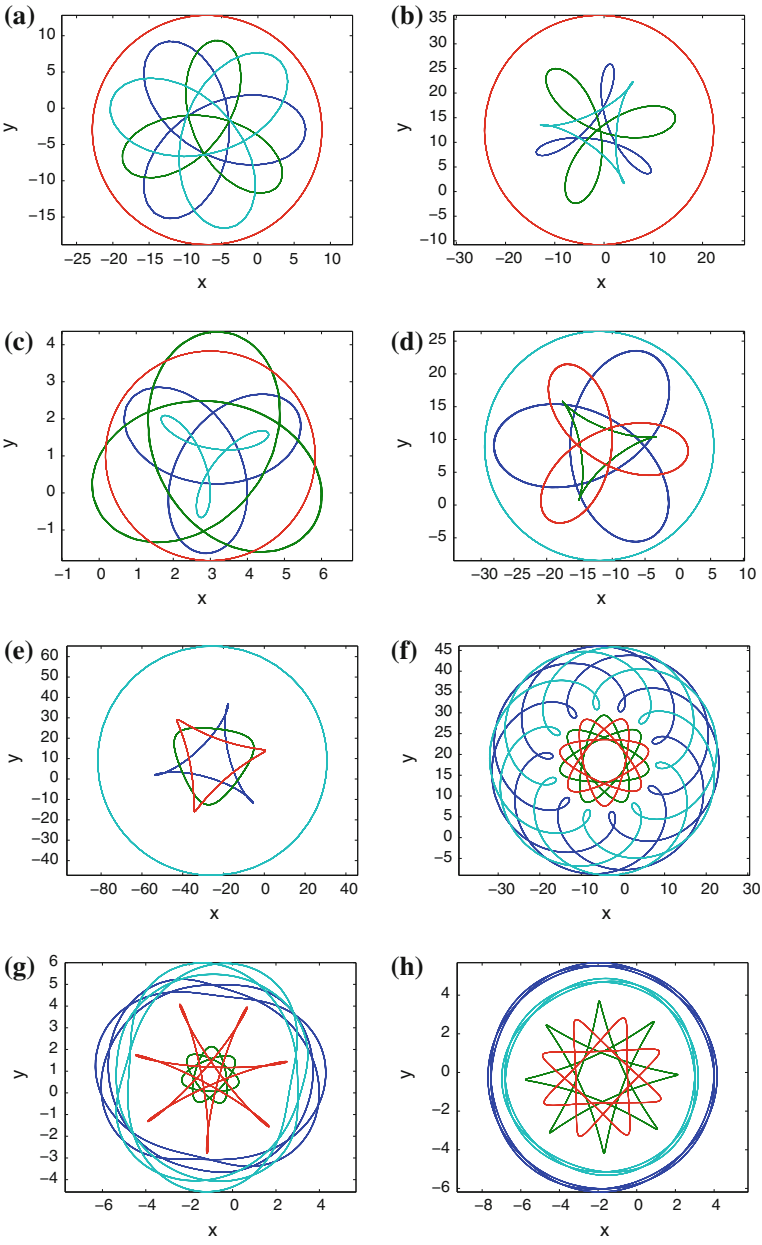

Fig. 6.12 Sample orbits with four agents using the extended consensus protocol; complete graph. **a**–**c** $B = \text{diag}(-1, -1, +1, -1)$, **d** and **e** $B = \text{diag}(-2, -2, -2, 2)$, **f** $B = \text{diag}(5, -2, -2, 5)$, **g** $B = \text{diag}(5, -0.866, -3.208, 5)$, **h** $B = \text{diag}(3.229, -2, -1.515, 5)$

where $\mathbb{S}^1 = \{(x, y) \in \mathbb{R}^2 : x^2 + y^2 = 1\}$ is the equator. The geodesic projection creates larger distortions of distances near the equator.

Figure 6.14 shows the results by applying the geodesic projection on a surface of revolution. The "vase" shown in this figure was generated using the parametric equations

$$x = (2 + \cos u) \sin v, \qquad y = (2 + \cos u) \cos v, \qquad z = u, \tag{6.25}$$

where u and v are the local coordinates on the two-dimensional vase manifold. Although not as elaborate or elegant as the vases of the Greek geometric period shown in Fig. 6.14, one nonetheless cannot help but admire the richness of the geometric patterns shown in Fig. 6.14, generated by the simple control law (6.10).

6.9 Discussion: The Mathematics of Aesthetics

An often repeated dictum of common wisdom is that "beauty is in the eye of the beholder." But is it? Although it is clear that perception of appeal or beauty is mainly an objective process (no ontological esthetic feeling is known), it is also equally clear that there exist esthetically attractive visual stimuli that transcend personal taste and seem to invoke the same feelings of acceptance or pleasure (equivalently, distastefulness or displeasure) among the majority of human observers. Several psychological studies seem to indicate that the human visual perception system is wired to be drawn to (overt or covert) symmetric, orderly patterns [4, 23, 24]. Plato (427–347 BC) was the first to state that "balanced things are always beautiful." Besides, isn't true that the creative artistic process, in general, produces order from disorder? If symmetry and order is the embodiment of harmony and beauty, and their lack is the manifestation of the opposite[2] (the constant struggle between χάος and κόσμος in ancient Greek culture) shouldn't perhaps be possible to describe certain esthetics using formal methods?

In his influential essay *Inquiry into the Origin of Our Ideas of Beauty and Virtues* the British philosopher Francis Hutcheson (1694–1746) attempted to answer this question, by showing how beauty depends on formal qualities. He suggested that beauty is "uniformity amidst variety." Thus, according to Hutcheson, richly varied compositions that are organized in accordance with some underlying unifying principle are beautiful [28]. The contemporary theory of the psychology of esthetics actually replaces the prominence of classical symmetry with the somewhat similar, albeit vague, notion of "organic unity" [33].

[2] Not everyone is in agreement, of course, with the classical notion of beauty and symmetry. One can easily argue that nonsymmetric patterns may also be esthetically pleasing as long as they do not result in chaos [26]. Recent psychological studies of works of modern art actually claim that it is the cognitive processes themselves that are involved in understanding, classifying, and evaluating a work of art which determine positive, self-rewarding esthetic experiences [20]. Even so, good gestalts tend to give preference to symmetry over nonsymmetry [13].

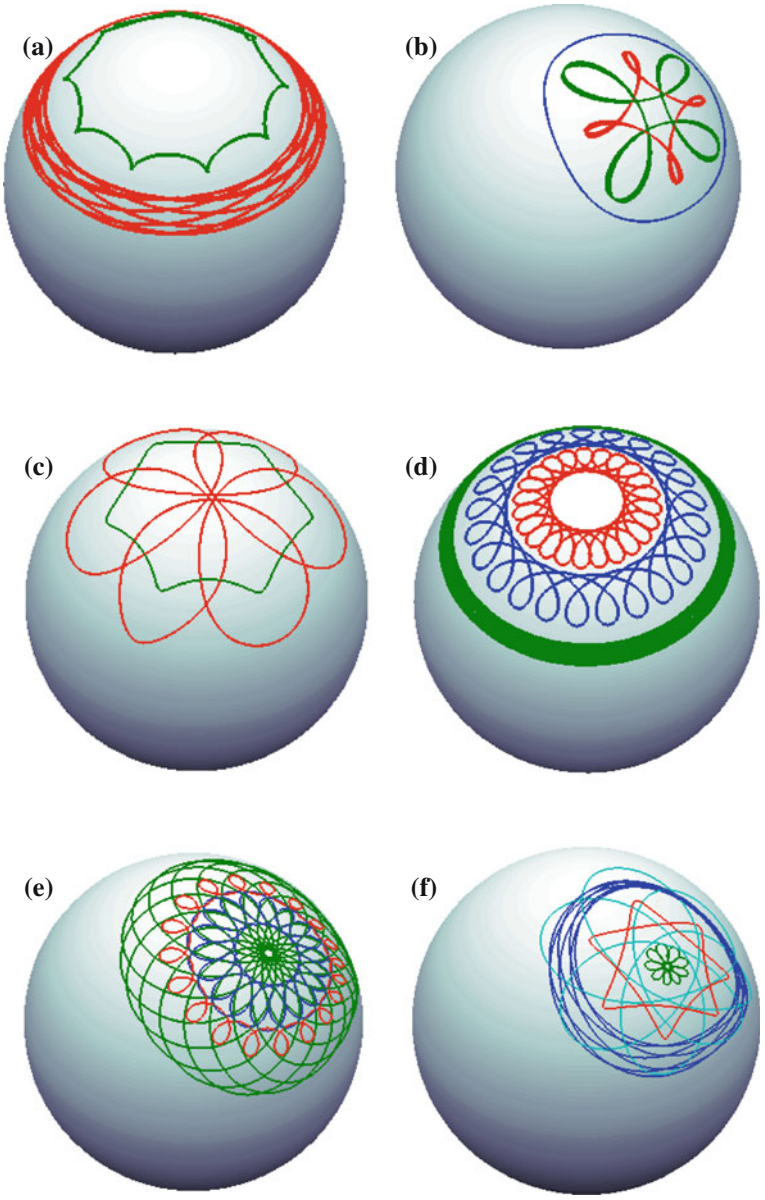

Fig. 6.13 *Sample orbits* on a *sphere* with three [(**a**)–(**d**)] and four [(**e**)–(**f**)] agents using the extended consensus protocol; path graph. **a** and **c** $B = \text{diag}(0, 1, -6.5933)$, **b** $B = \text{diag}(-2.4736, 3, 2)$, **d** $B = \text{diag}(1, -2.9054, 0.5)$, **e** $B = \text{diag}(1, 2, 2.0034, -1)$, **f** $B = \text{diag}(2, 0.1826, 0.6126, 2)$

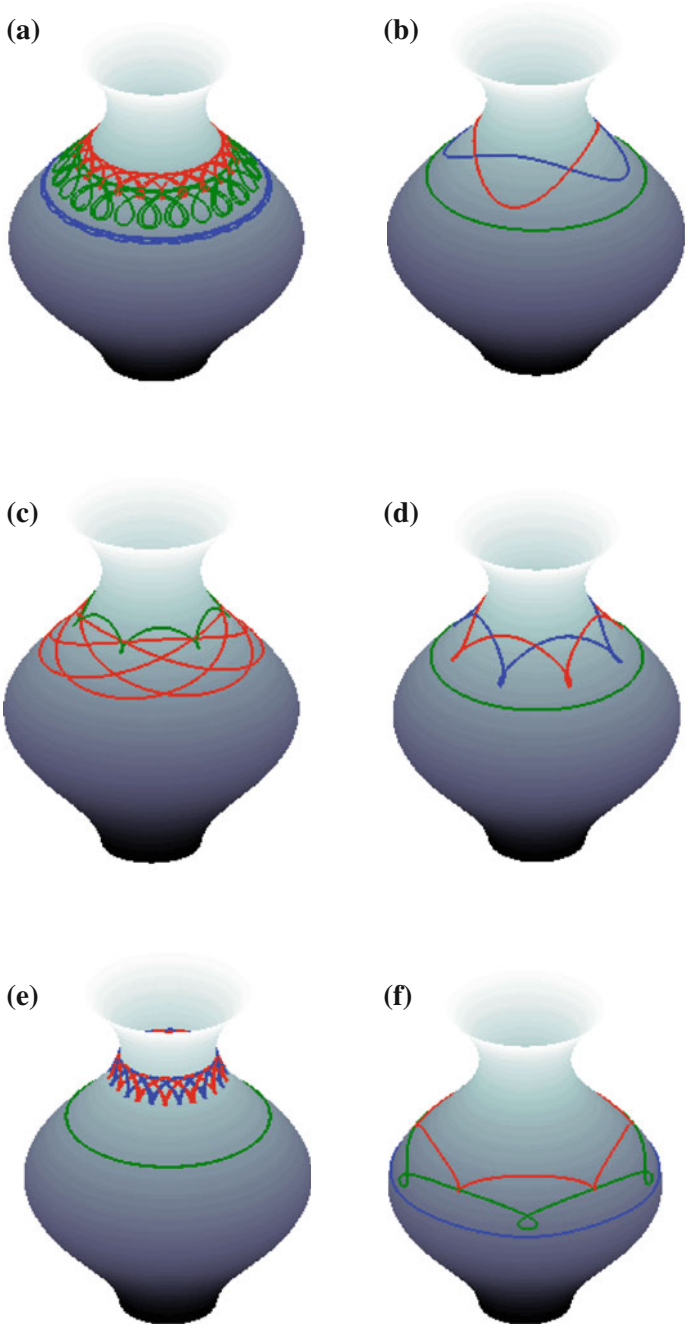

Fig. 6.14 *Sample orbits* on a *vase* with three agents using the extended consensus protocol; path graph. **a** $B = \text{diag}(-2.4736, 3, 2)$, **b** $B = \text{diag}(4, -4, 4)$, **c** $B = \text{diag}(0, 1, -6.5933)$, **d** $B = \text{diag}(-1, 2, -1)$, **e** $B = \text{diag}(1, -8.7289, 1)$, **f** $B = \text{diag}(1, -1, -0.5)$,

Motivated by such observations, the American mathematician G. Birkhoff (1884–1944) introduced the concept of an *esthetic measure*, a single number that describes the esthetic appeal of an object [3]. Since then, several versions and modifications of Birkhoff's original esthetic measure have been proposed, all of which defining the esthetic measure—in one form or another—as the ratio of order over disorder, equivalently, symmetry over complexity.

More formally, Birkhoff's esthetic measure M is defined by

$$M = \frac{O}{C}, \tag{6.26}$$

where O is the order or harmony of the observed work, and C is the object's complexity. As also Birkhoff himself recognized, formalizing these concepts, which depend on the context, biases of the observer, and so on, is difficult. Whereas there is a consensus among researchers that O is essentially a measure of the object's symmetries, there seems to be less of an agreement on how one measures its complexity. One proposal that has come forth is that C is related to the redundant information conveyed [2, 29]. This has given rise to several information-theoretic measures ("informational aesthetics measures") based on Kolmogorov complexity, Shannon's information theory and physical entropy [41]. The field of computational esthetics has evolved around these ideas in an effort to define and quantify artistic creativity using mathematical algorithms [48].

What does the field of computational esthetics have to do with control theory? In this work we have shown that control algorithms can be used to generate geometric patterns in a natural manner. Is not difficult for one to envision generalizations leading to more complicated art forms. Most importantly, recall that a large part of control theory deals with the maximization of a given payoff. In this context, it would be intriguing to investigate control algorithms that attempt to maximize the esthetic measure within a given class.

6.10 Conclusions

We have presented an extension of the classical consensus algorithm for multi-agent systems to achieve consensus outside the convex hull of the initial conditions of the agents. As a by-product of this idea, we have shown how to generate agent trajectories leading to intricate geometric patterns in the plane using only relative, local information. Future work will concentrate on developing a general theory for orbit design for an arbitrary number of agents in two, and three dimensions. Apart from their inherent esthetical appeal, these orbits can have immediate applications in the area of coordinated, persistent surveillance and monitoring using a team of agents interacting using local information. An interesting lingering question that still remains to be answered, is whether one can classify these curves according to their esthetic appeal using a properly defined esthetic measure.

Acknowledgments The authors would like to thank Magnus Egerstedt and Amy LaViers for organizing the session on "Controls and Art" during the 2011 American Control Conference and for inviting the authors of this paper to contribute to the session. The authors would also like to thank Prof. Athanassios Economou from the College of Architecture at Georgia Tech for several informative discussions over the use of group symmetries in art and architecture.

References

1. Arcak M (2007) Passivity as a design tool for group coordination. IEEE Trans Autom Control 52(8):1380–1390
2. Bense M (1969) Einführung in die informationstheoretische Asthetik. Grundlegung und Anwendung in der Texttheorie. Rowohlt Taschenbuch Verlag, Hamburg
3. Birkhoff GD (1933) Aesthetic measure. Harvard University Press, Cambridge
4. Bouleau C (1980) The painter's secret geometry: a study of composition in art. Hacker Art Books, New York
5. Boyer CB (1968) A history of mathematics. Wiley, New York
6. Brewer J (1978) Kronecker products and matrix calculus in system theory. IEEE Trans Circ Syst 25(9):772–781
7. Coldstream JN (2003) Geometric Greece: 900–700 BC. Psychology Press, Abingdon
8. Dawson I (2013) Spirographs. http://www.iandawson.net/spiro.php. Accessed 20 May 2013
9. Economou A (2011) The symmetry lessons from Froebel building gifts. Environ Plann B: Plann Des 26(1):75–90
10. El-Said I, El-Bouri T, Critchlow K, Damlūjī SS (1993) Islamic art and architecture: the system of geometric design. Garnet Publishing, London
11. Ettinghausen R, Grabar O, Jenkins M (2001) Islamic art and architecture: 650–1250, vol 51. Yale University Press, London
12. Fax JA, Murray RM (2004) Information flow and cooperative control of vehicle formations. IEEE Trans Autom Control 49(9):1465–1476
13. Frith CD, Nias DKB (1974) What determines aesthetic preferences? J Gen Psychol 91:163–173
14. Godsil CD, Royle G (2001) Algebraic graph theory. Springer, New York
15. Grünbaum B, Grünbaum Z, Shepard GC (1986) Symmetry in moorish and other ornaments. Comput Math Appl 12(3):641–653
16. Hall LM (1992) Trochoids, roses, and thorns-beyond the spirograph. Coll Math J 23(1):20–35
17. Halliwell L (2013) http://www.lesleyhalliwell.co.uk/. Accessed 20 May 2013
18. Knight TW (1995) Transformations in design: a formal approach to stylistic change and innovation in the visual arts. Cambridge University Press, Cambridge
19. Lawrence JD (1972) A catalog of special plane curves. Dover Publications, New York
20. Leder H, Belke B, Oeberst A, Augustin D (2004) A model of aesthetic appreciation and aesthetic judgments. Br J Psychol 95(4):489–508
21. Leonard NE, Fiorelli E (2001) Virtual leaders, artificial potentials, and coordinated control of groups. 40th IEEE Conference on Decision and Control, pp 2968–2973, 4–7 Dec 2001
22. Leonard NE, Young GF, Hochgraf K, Swain DT, Trippe A, Chen W, Fitch K, Marshall S (2014) Controls and art. In the dance studio: an art and engineering exploration of human flocking. In: Lecture Notes in Computer Sciences. Springer-Verlag, New York, p xxx
23. Locher P, Nodine C (1989) The perceptual value of symmetry. Comput Math Appl 17(4):475–484
24. Locher P, Nodine C (1987) Eye movements: from physiology to cognition. Chapter Symmetry Catches the Eye. Elsevier, Holland, pp 353–361
25. Marshall JA, Broucke ME, Francis BA (2004) Formations of vehicles in cyclic pursuit. IEEE Trans Autom Control 49(11):1963–1974
26. McManus C (2005) Symmetry and asymmetry in aesthetics and the arts. Eur Rev 13:157–180

27. Mesbahi M, Egerstedt M (2010) Graph theoretic methods in multiagent networks. Princeton University Press, Princeton
28. Mitchell WJ (1990) The logic of architecture: design, computation, and cognition. MIT Press, Cambridge
29. Moles A (1968) Information theory and esthetic perception. University of Illinois Press, Champaign
30. Olfati-Saber R (2006) Swarms on sphere: a programmable swarm with synchronous behaviors like oscillator networks. In: 45th IEEE Conference on Decision and Control, pp 5060–5066
31. Olfati-Saber R, Murray RM (2004) Consensus problems in networks of agents with switching topology and time-delays. IEEE Trans Autom Control 49(9):1520–1533
32. Olfati-Saber R, Fax JA, Murray RM (2006) Consensus and cooperation in multi-agent networked systems. Proc IEEE 97:215–233
33. Osborne H (1986) Symmetry as an aesthetic factor. Comput Math Appl 12(1):77–82
34. Parchos EA, Sotiroudis P (1999) The schemata of the stars: Byzantine astronomy from A.D. 1300. World Scientific, Singapore
35. Park J-H, Joo Y, Yang J-G (2007) Cycloids in Louis I. Kahns Kimbell Art Museum at Fort Worth, Texas. Math Intell 29:42–48
36. Pavone M, Frazzoli E (2007) Decentralized policies for geometric pattern formation and path coverage. J Dyn Syst Meas Contr 129:633–643
37. Pohl D (2013) The loop yoga drawing project. http://spirographart.blogspot.com/. Accessed 20 May 2013
38. Public domain image "File:Triquetra_on_book_cover.jpg" from user Chameleon on the Wikimedia Commons. http://commons.wikimedia.org/wiki/File:Triquetra_on_book_cover.jpg;. Accessed 10 Sept 2013
39. Public domain image ID 289442_WDC25C21 (acquisition date 01 Sept 2005). United States Geological Survey. http://earthexplorer.usgs.gov/;. Accessed 21 Nov 2013
40. Ren W, Beard RW (2005) Consensus seeking in multi-agent systems using dynamically changing interaction topologies. IEEE Trans Autom Control 50(5):655–661
41. Rigau J, Feixas M, Sbert M (2008) Informational aesthetics measures. IEEE Comput Graph Appl 28(2):24–34
42. Sarlette A, Sepulchre R (2009) Consensus optimization on manifolds. SIAM J Control Optim 48(1):56–76
43. Schattschneider D, Hofstadter D (2004) In: Escher MC (ed) Visions of symmetry. Thames & Hudson, London
44. Schoelling AP, Siegel H, Augugliaro F, D'Andrea R (2014) Controls and art. So you think you can dance? Rhythmic flight performances with quadrocopters. In: Lecture Notes in Computer Sciences. Springer-Verlag, New York, p xxx
45. Schweitzer B (1971) Greek geometric art. Phaidon, London
46. Simmons Jeffrey. Paintings: 1999–2000: Trochoid. http://jeffreysimmonsstudio.com/project/trochoids-paintings-1999/. Accessed 20 May 2013
47. Simoson AJ (2008) Albrecht Dürer's trochoidal woodcuts. Probl Resour Issues Math Undergraduate Stud (PRIMUS) 18(6):489–499
48. Stiny G, Gips J (1978) Algorithmic aesthetics: computer models for criticism and design in the arts. University of California Press, Berkeley
49. Suzuki I, Yamashita M (1999) Distributed anonymous mobile robots: formation of geometric patterns. SIAM J Comput 28(4):1347–1363
50. Tron R, Afsari B, René Vidal (2012) Riemannian consensus for manifolds with bounded curvature. IEEE Trans Autom Control
51. Tsiotras P, Reyes Castro LI. A note on the consensus protocol with some applications to agent orbit pattern generation. In: 10th Symposium on Distributed Autonomous Robotic Systems (DARS). Lausanne, Switzerland, 1–3 Nov 2010
52. Wang L-S, Krishnaprasad PS (1992) Gyroscopic control and stabilization. J Nonlinear Sci 2:367–415
53. Wessén E (1952) Det svenska runverket. http://fornvannen.se/pdf/1950talet/1952_193.pdf (in Swedish)
54. Weyl H (1952) Symmetry. Princeton University Press, London